Electronic Supplementary Information (ESI)

Effect of cysteine thiols on the catalytic and anticancer activity of Ru(II) sulfonyl-ethylenediamine complexes

Feng Chen, Isolda Romero-Canelón, Abraha Habtemariam, Ji-Inn Song, Samya Banerjee, Guy J. Clarkson, Lijiang Song, Ivan Prokes and Peter J. Sadler

Contents

Reference

Ligand Synthesis

N-(2-(benzylamino)ethyl)-4-nitrobenzenesulfonamide (4-NO_2-phenyl-SO_2-EnBz).[1] A solution of N-benzylethylenediamine (0.214 mL, 1.43 mmol) in DCM (100 mL) was placed in a round-bottom flask. A solution of 4-nitrobenzenesulfonyl chloride (0.3 g, 1.36 mmol) in DCM (50 mL) was added slowly via a dropping funnel, and the mixture was stirred vigorously for 12 h. The solvent was removed on a rotary evaporator and the product further purified on a silica gel column (10% MeOH and 90% DCM) to give a white solid. Yield = 246 mg (54%). **^{1}H NMR** (400 MHz, $CDCl_3$): δ_H 2.73 (t, *J* = 5.8 Hz, 2H), 3.05 (t, *J* = 5.8 Hz, 2H), 3.67 (s, 2H), 7.21 (d, *J* = 6.8 Hz, 2H), 7.28-7.33 (m, 3H), 7.99 (d, *J* = 8.9 Hz, 2H), 8.30 (d, *J* = 8.6 Hz, 2H); ESI-MS: *Calc* for $[C_{15}H_{17}N_3O_4S + H]^+$ 336.1 m/z, found: 335.9 m/z.

N-(2-(benzylamino)ethyl)benzenesulfonamide (phenyl-SO_2-EnBz). A solution of N-benzylethylene diamine (0.50 mL, 3.33 mmol) in dichloromethane (100 mL) was placed in a round-bottom flask. A solution of benzenesulfonyl chloride (0.212 mL, 1.664 mmol) in DCM (50 mL) was added slowly via a dropping funnel, and the mixture was stirred vigorously for 12 h. The solvent was removed on a rotary evaporator and the product further purified on a silica gel column (10% MeOH and 90% DCM) to get white solid. Yield = 323 mg (67%). **^{1}H NMR** (400 MHz, $CDCl_3$): δ_H 2.67 (t, *J* = 5.8 Hz, 2H), 3.00 (t, *J* = 5.8 Hz, 2H), 3.62 (s, 2H), 7.19-7.21 (m, 2H), 7.22-7.24 (m, 1H), 7.28-7.31 (m, 2H), 7.45-7.48 (m, 2H), 7.52-7.56 (m, 1H), 7.82-7.85 (m, 2H); ESI-MS: *Calc* for $[C_{15}H_{18}N_2O_2S + H]^+$ 291.1 m/z, found: 290.8 m/z.

N-(2-(benzylamino)ethyl)-4-fluorobenzenesulfonamide (4-F-phenyl-SO_2-EnBz). A solution of N-benzyl ethylenediamine (0.278 mL, 1.85 mmol) in dichloromethane (100 mL) was placed in a round-bottom flask. A solution of 4-fluorobenzenesulfonyl chloride (0.3 g, 1.54 mmol) in DCM (50 mL) was added slowly via a dropping funnel, and the mixture was stirred vigorously for 12 h. The solvent was removed on a rotary evaporator and the product further

purified on a silica gel column (10% MeOH and 90% DCM) to give a white solid. Yield = 270 mg (57%). **^{1}H NMR** (400 MHz, $CDCl_3$): δ_H 2.71 (t, *J* = 5.8 Hz, 2H), 3.00 (t, *J* = 5.8 Hz, 2H), 3.66 (s, 2H), 7.15 (t, *J* = 8.6 Hz, 2H), 7.22 (d, *J* = 6.9 Hz, 2H), 7.28-7.33 (m, 2H), 7.83-7.86 (m, 2H); ESI-MS: *Calc* for $[C_{15}H_{17}FN_2O_2S + H]^+$ 309.1 m/z, found: 308.8 m/z.

N-(2-(benzylamino)ethyl)-5-(dimethylamino)naphthalene-1-sulfonamide (DsEnBz). A solution of N-benzylethylenediamine (0.267 mL, 1.78 mmol) in dichloromethane (100 mL) was placed in a round-bottom flask. A solution of dansyl chloride (400 mg, 1.483 mmol) in DCM (50 mL) was added slowly via a dropping funnel, and the mixture was stirred vigorously for 12 h. The solvent was removed on a rotary evaporator and the product further purified on a silica gel column (6% MeOH and 94% DCM) to give a white solid. Yield = 324 mg (57%). **^{1}H NMR** (400 MHz, MeOD-d_4): δ_H 2.51 (t, *J* = 6.2 Hz, 2H), 2.87 (s, 6H), 2.99 (t, *J* = 6.2 Hz, 2H), 3.46 (s, 2H), 7.09 (d, *J* = 6.6 Hz, 2H), 7.20-7.28 (m, 4H), 7.55-7.60 (m, 2H), 8.21 (dd, *J* = 0.92 Hz, 7.2 Hz, 2H), 8.33 (d, *J* = 8.6 Hz, 1H), 8.56 (d, *J* = 8.5 Hz, 1H); ESI-MS: *Calc* for $[C_{21}H_{26}N_3O_2S + H]^+$ 384.1 m/z, found: 384.2 m/z.

Table S1. Crystallographic data for complex **3**.

Crystal character	Red block
Empirical formula	$C_{28}H_{29}IN_2O_2RuS$
Formula weight	685.56
Temp (K)	150(2)
Crystal system	monoclinic
Space group	P_n
a/Å	10.91549(4)
b/Å	9.33603(4)
c/Å	13.28373(5)
α/°	90
β/°	98.2296(3)
γ/°	90
Volume/Å^3	1339.768(9)
Z	2
D_{calc}(mg/cm^3)	1.699
μ/mm^{-1}	14.728
F(000)	680.0
Crystal size/mm^3	0.6 × 0.16 × 0.08 orange block
Reflections collected	38933
Indep reflection	5343
R [I>=2σ (I)]	R^1 = 0.0168
Final R [all data]	R^2 = 0.0426
CCDC No.	2117792

Table S2. Selected hydrogen bond lengths (Å) and angle (º) for complex **3**.

D	H	A	d(D-H)/Å	d(H-A)/Å	d(D-A)/Å	D-H-A/°
N12	H12	I1	0.85(6)	2.83(5)	3.315(3)	118(4)

Table S3. MS peak assignments for products from reactions of complex **2** with GSH and NAC (10 mol equiv, MeOH/H_2O, 1: 9 (v/v), pH 7). Fore HPLC peak numbering, see Fig. S4; mass spectra shown in Figures S6 and S7.

Peak	Retention time (min)	Mass (m/z)	Assignment
p1	17.3	715.67	$[(\eta^6\text{-biph})_2Ru_2(GS)_3+4H]^{2+}$
p2	27.6	997.89	$[(\eta^6\text{-biph})_2Ru_2(NAC)_3]^+$
p3	31.6	305.20	ligand [TsEnBz]+H^+
p4	34.7	559.10	complex **2**, $[C_{28}H_{29}N_2O_2RuS]^+$

Table S4. Antiproliferative activity of complex **2** towards human A549 lung cancer and A2780 ovarian cancer cells with sequential administration of 1 mol equiv of GSH or NAC at various concentrations (5, 10 and 50 μM).[a]

Thiol addition	Cell line[a]	
	A549	A2780
	IC_{50} (μM)	
None (**2** alone)	13.5 ± 1.4	11.25 ± 0.08
GSH (5 μM)	22.4 ± 1.3	27.3 ± 0.5
GSH (10 μM)	22.9 ± 2.1	43.9 ± 3.5
GSH (50 μM)	>50	> 50
NAC (5 μM)	25.8 ± 0.9	n.d.
NAC (10 μM)	39.9 ± 0.3	n.d.
NAC (50 μM)	> 50	n.d.

[a] Data are shown as mean ± standard deviation (STD). GSH or NAC was added to cells first, followed by adding complex **2** (with 10 min); following SRB protocols, cell viability was assessed after 24 h incubation with Ru^{II} complexes and washing with PBS.

Table S5. Induction of ROS and superoxide determined by flow cytometry experiments on A2780 human ovarian cancer cells.

Complex	Population (%)			
	FITC-A-/PE-A+	FITC-A+/PE-A+	FITC-A+/PE-A-	FITC-A-/PE-A-
2	15.4 ± 0.6 ***	1.4 ± 0.2 ***	71.7 ± 1.7 ***	11.4 ± 1.4 ***
2+GSH (0.5 µM)	13.2 ± 0.6 ***	0.7 ± 0.1 **	70.3 ± 0.4 ***	15.8 ± 0.4 ***
2+GSH (5 µM)	5.2 ± 0.4 **	0.67 ± 0.15 **	86.3 ± 0.5 ***	7.8 ± 0.4 ***
Positive	0.66 ± 0.08 **	98.8 ± 0.3 ***	0.77 ± 0.15 ***	0 ***
Negative	2.97 ± 0.15	1.53 ± 0.06	9.3 ± 0.3	86.2 ± 0.5

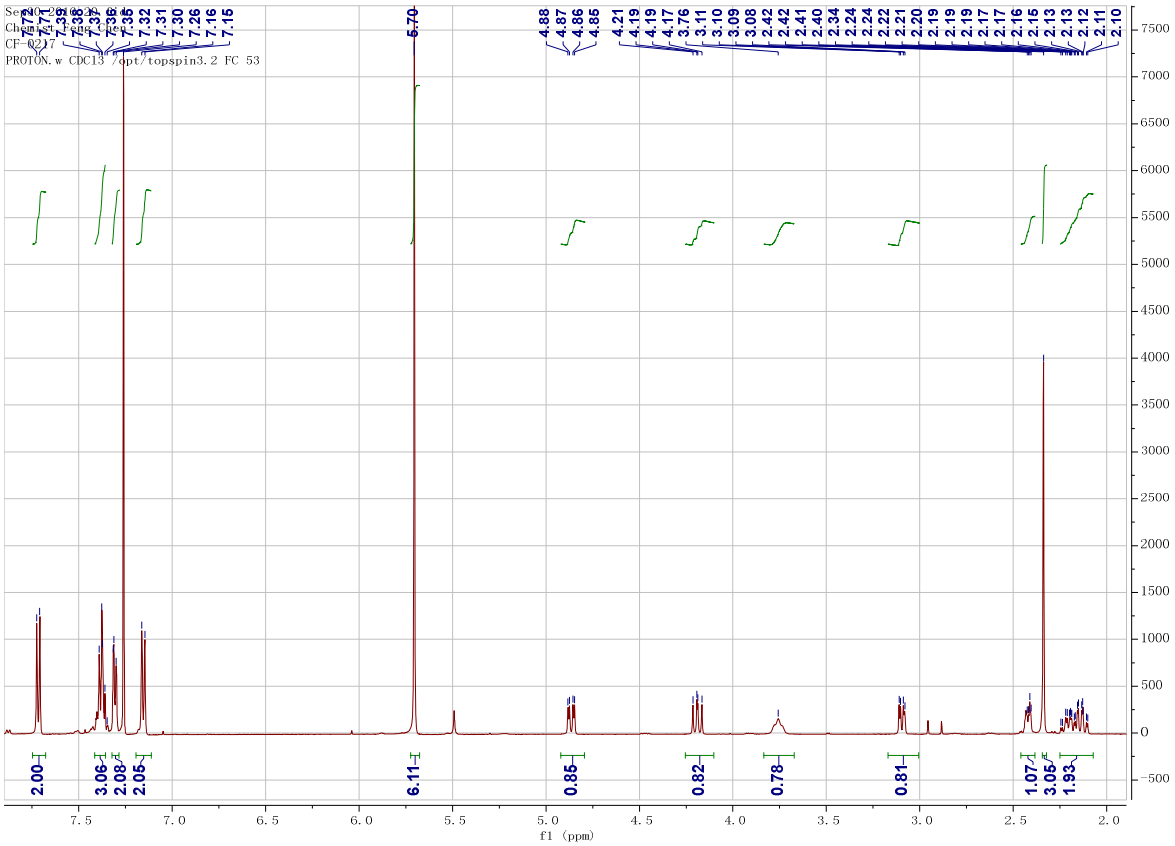

Figure S1. ^{1}H NMR spectrum of complex **1**

Figure S2. ^{13}C NMR spectrum of complex **1**

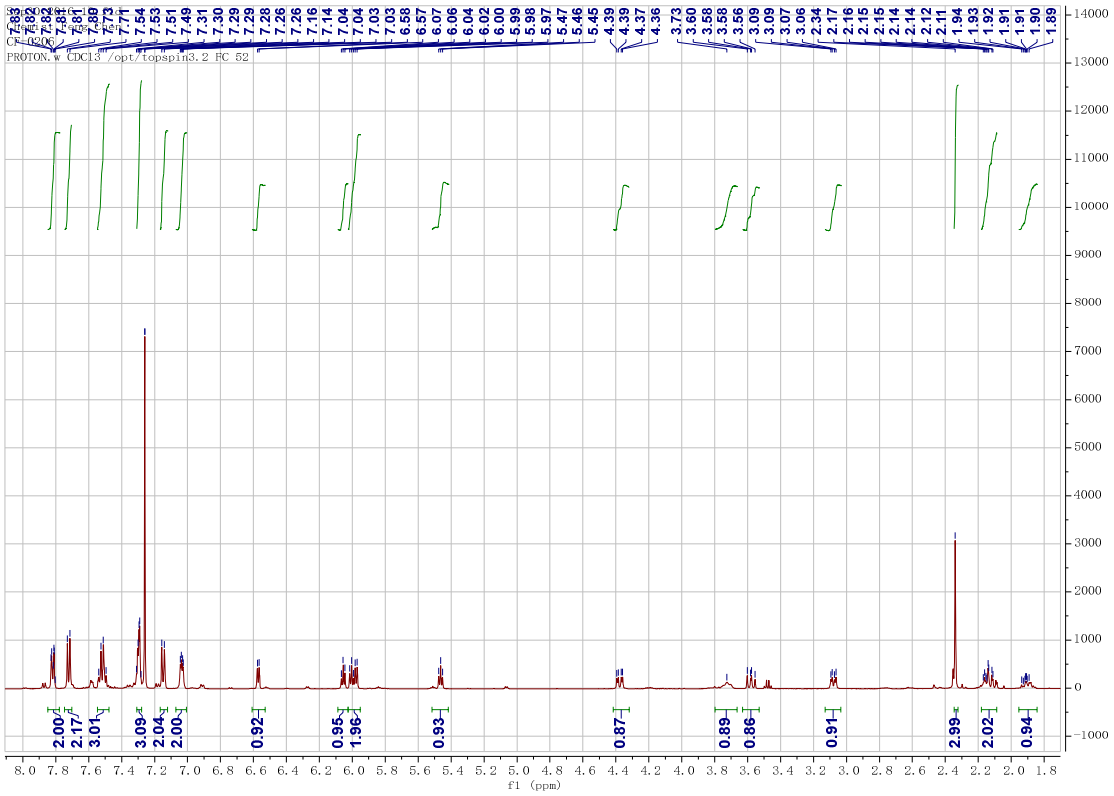

Figure S3. ^{1}H NMR spectrum of complex **2**

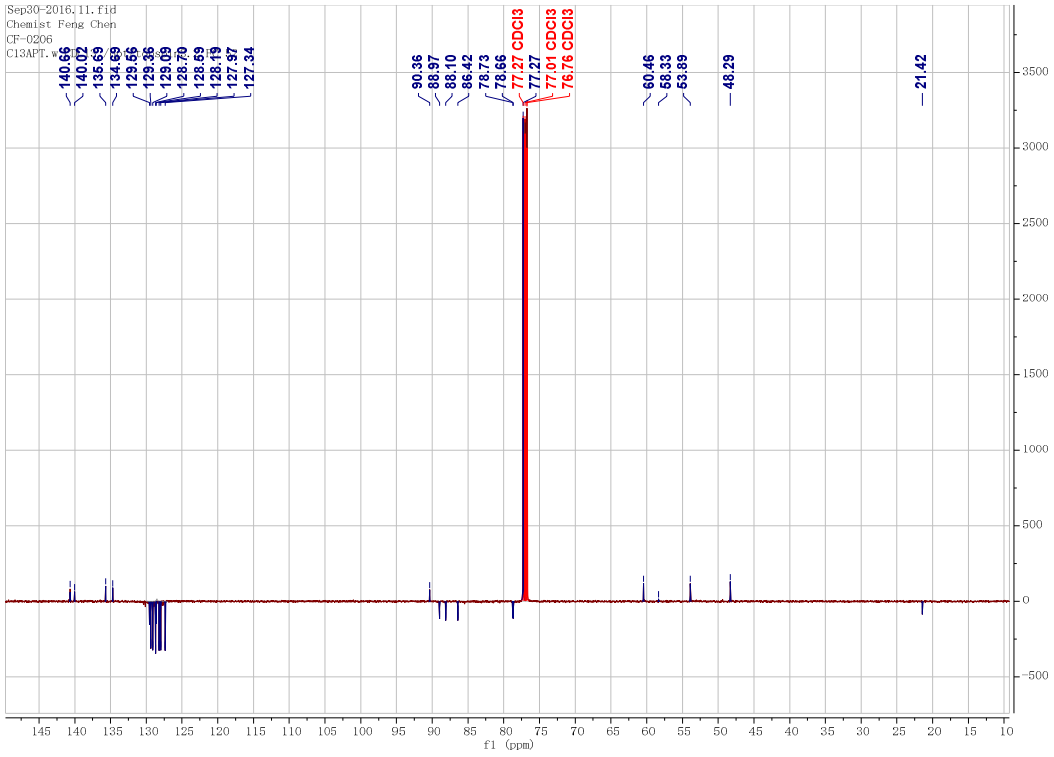

Figure S4. ^{13}C NMR spectrum of complex **2**

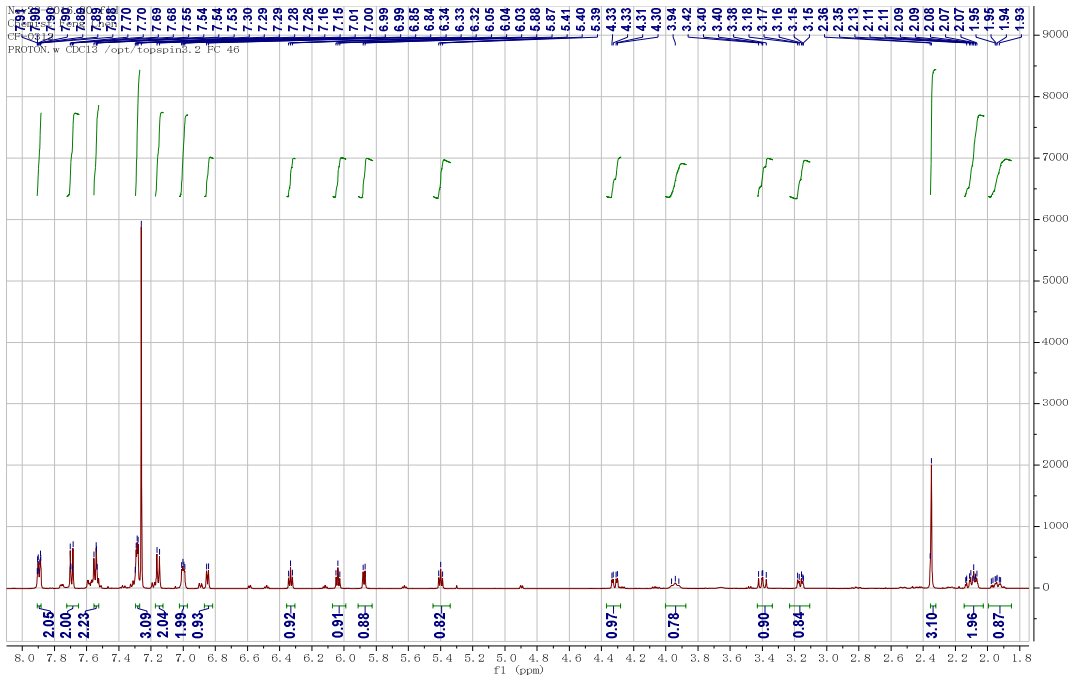

Figure S5. ^{1}H NMR spectrum of complex **3**

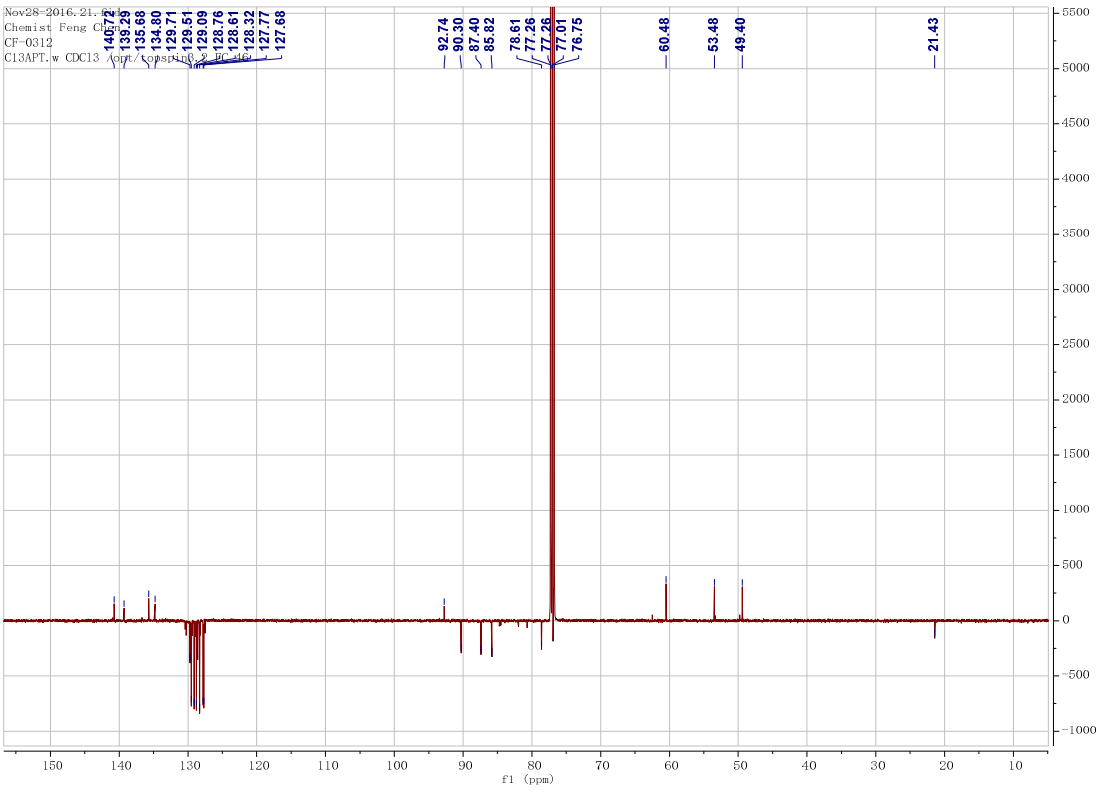

Figure S6. ^{13}C NMR spectrum of complex **3**

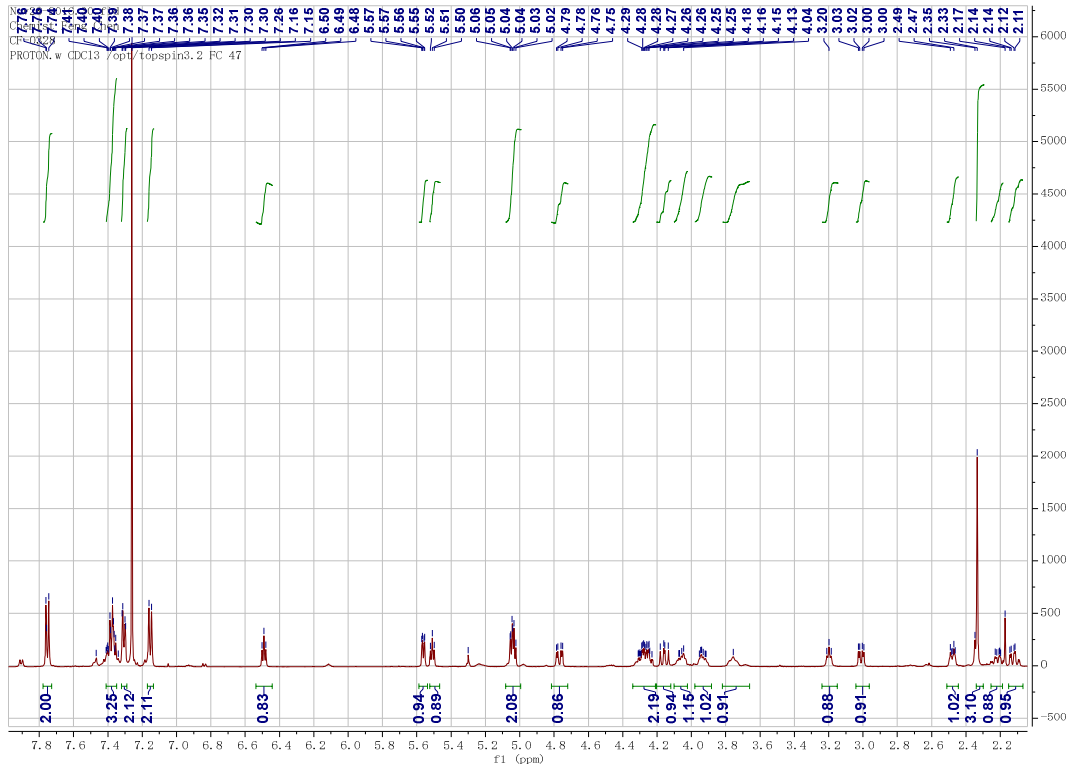

Figure S7. ^{1}H NMR spectrum of complex **4**

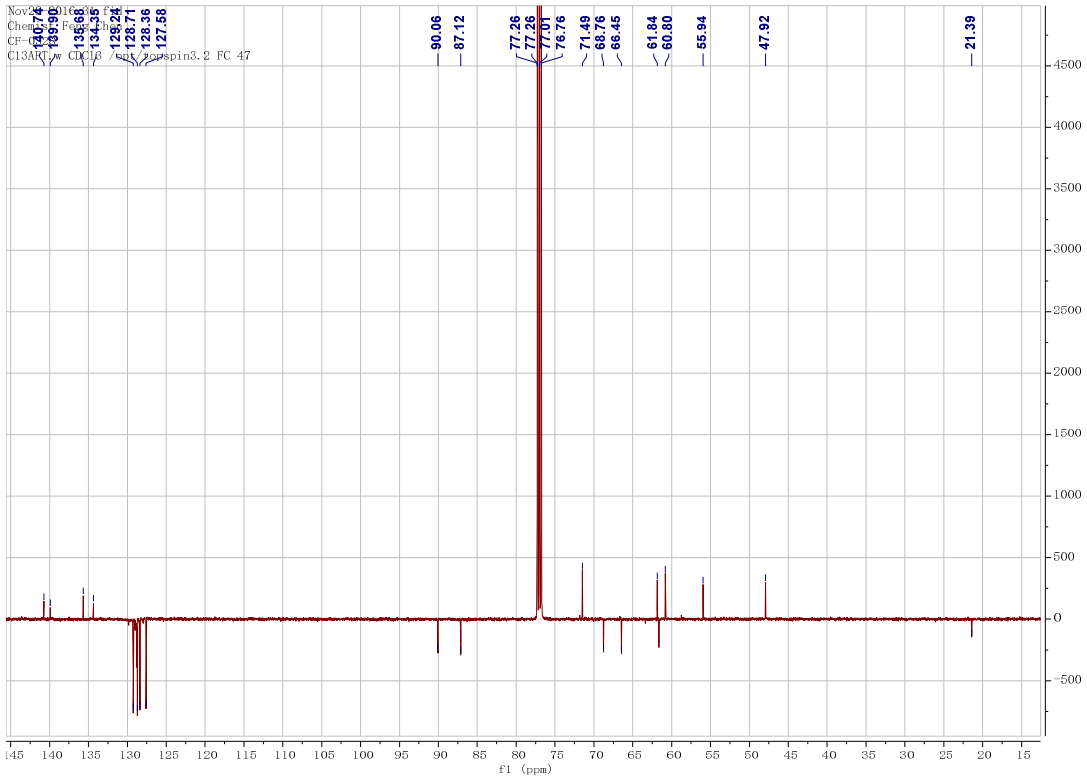

Figure S8. ^{13}C NMR spectrum of complex **4**

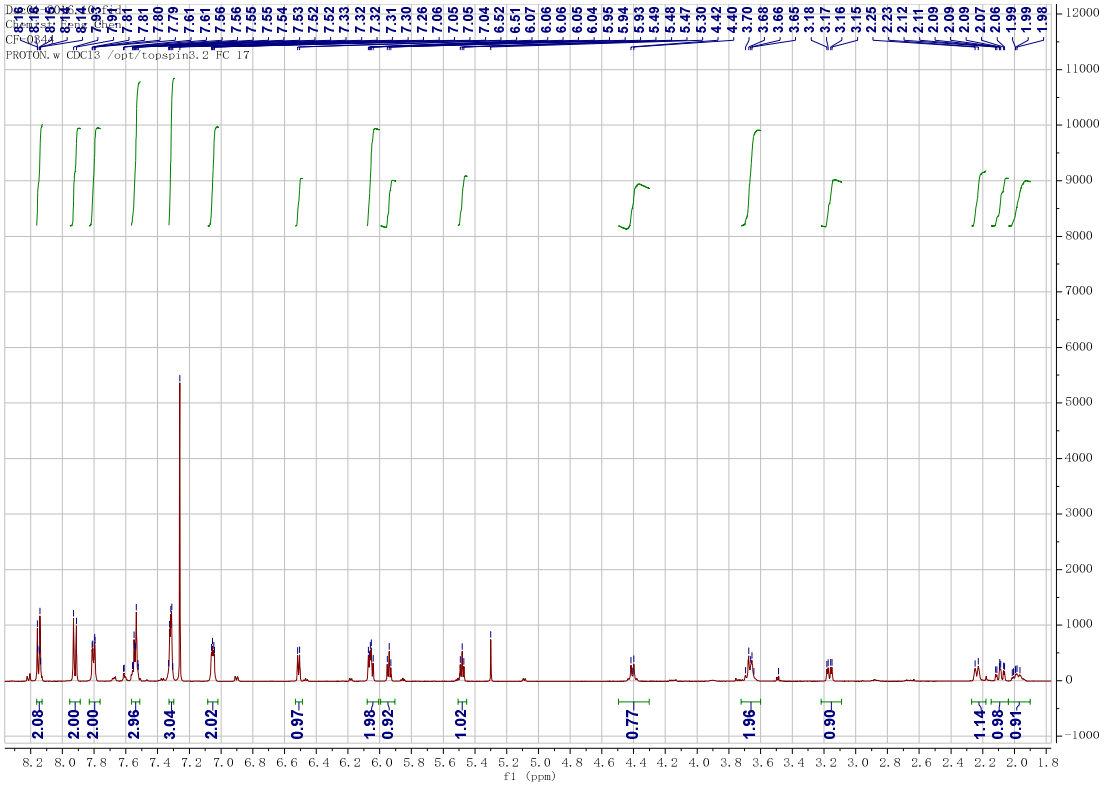

Figure S9. ^{1}H NMR spectrum of complex **5**

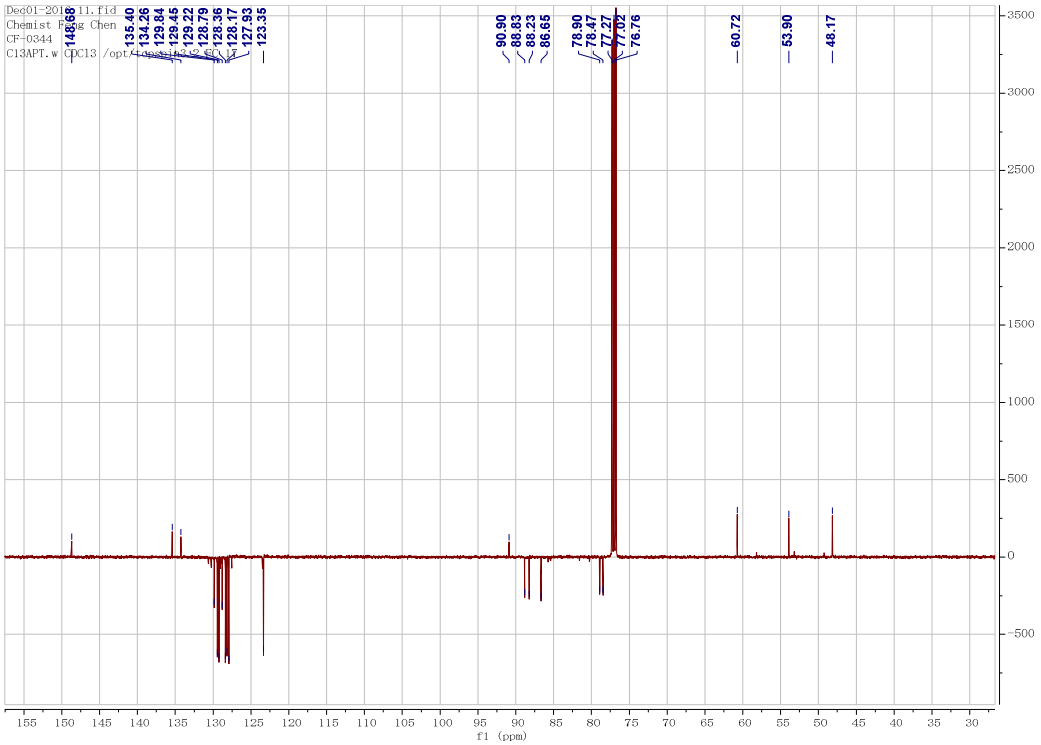

Figure S10. ^{13}C NMR spectrum of complex **5**

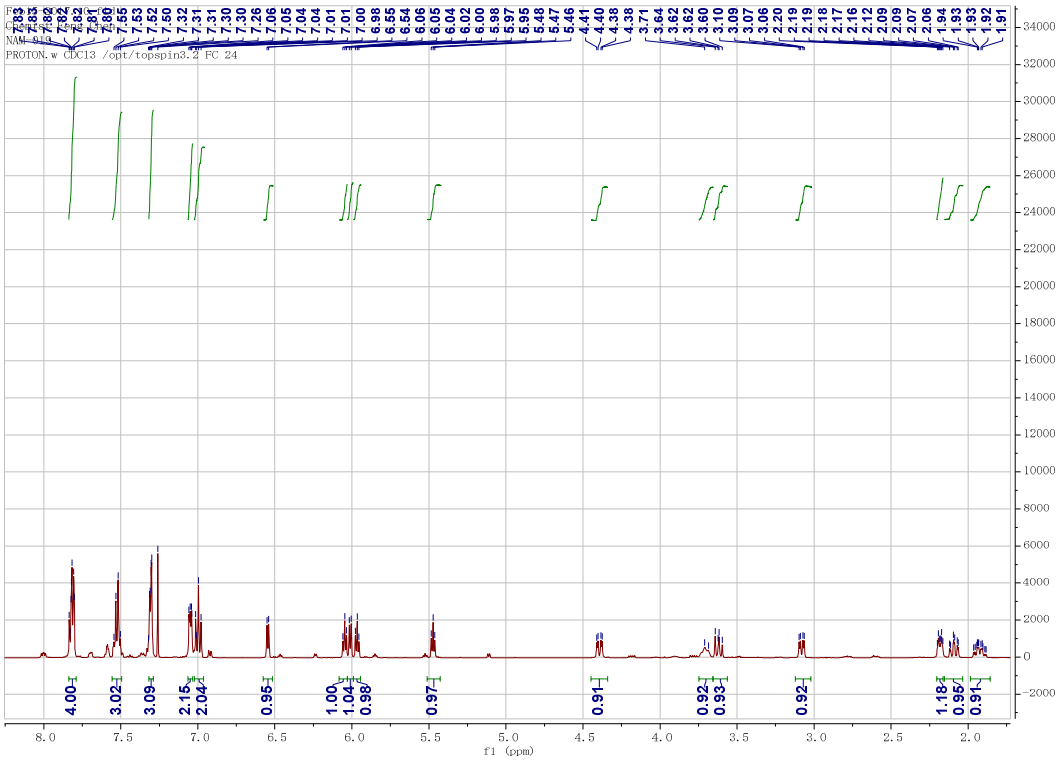

Figure S11. ^{1}H NMR spectrum of complex **6**

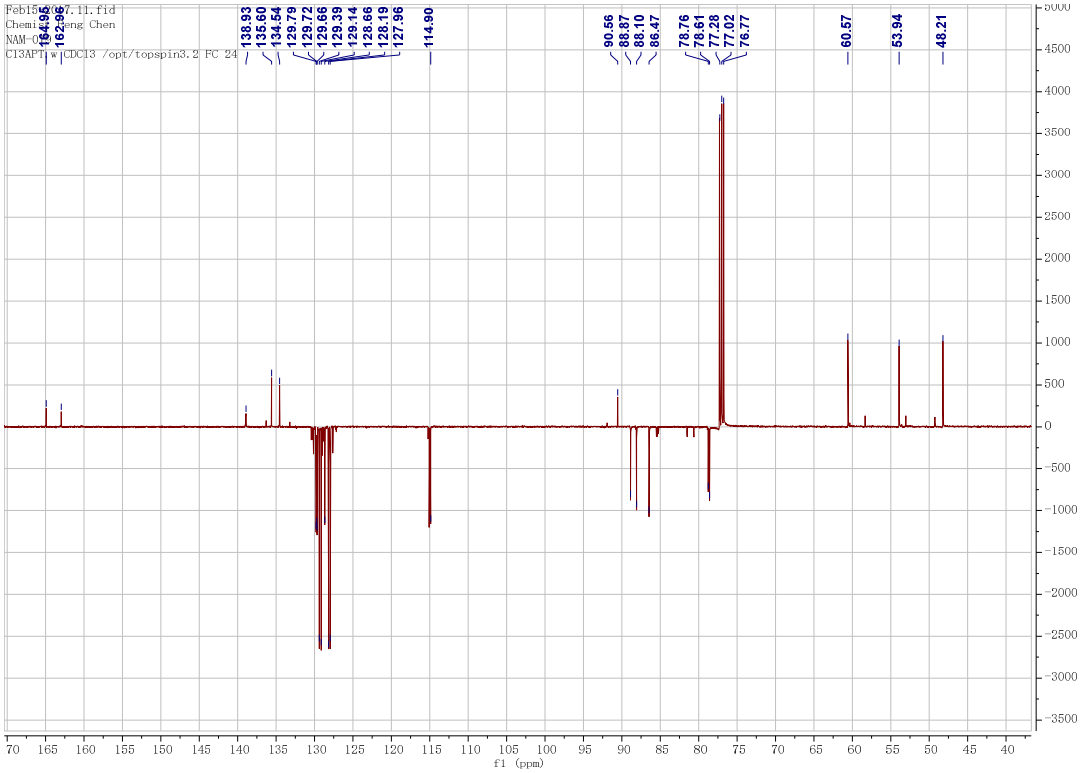

Figure S12. ^{13}C NMR spectrum of complex **6**

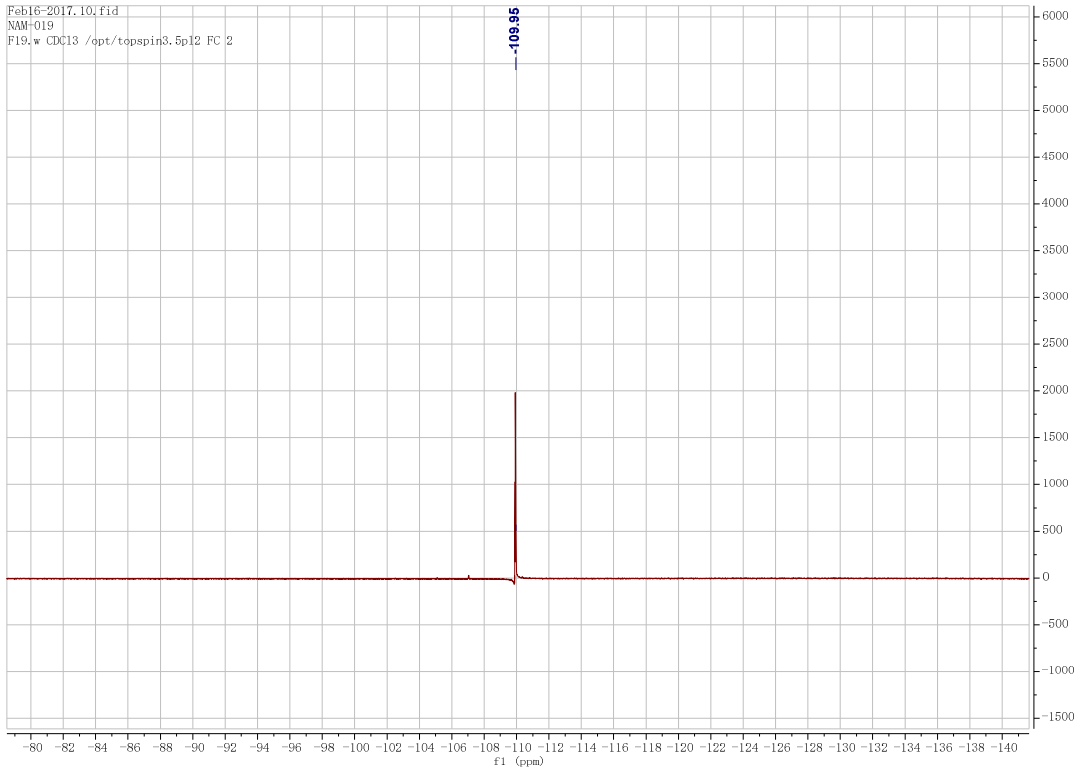

Figure S13. ^{19}F NMR spectrum of complex **6**

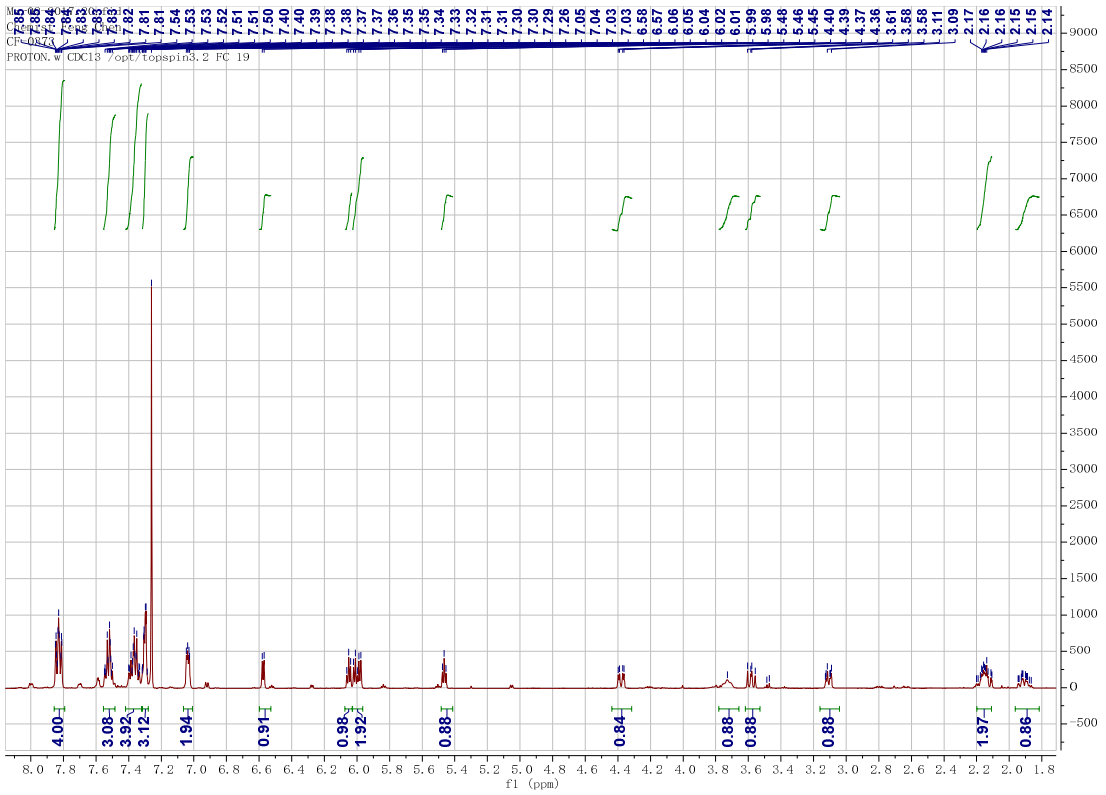

Figure S14. ^{1}H NMR spectrum of complex **7**

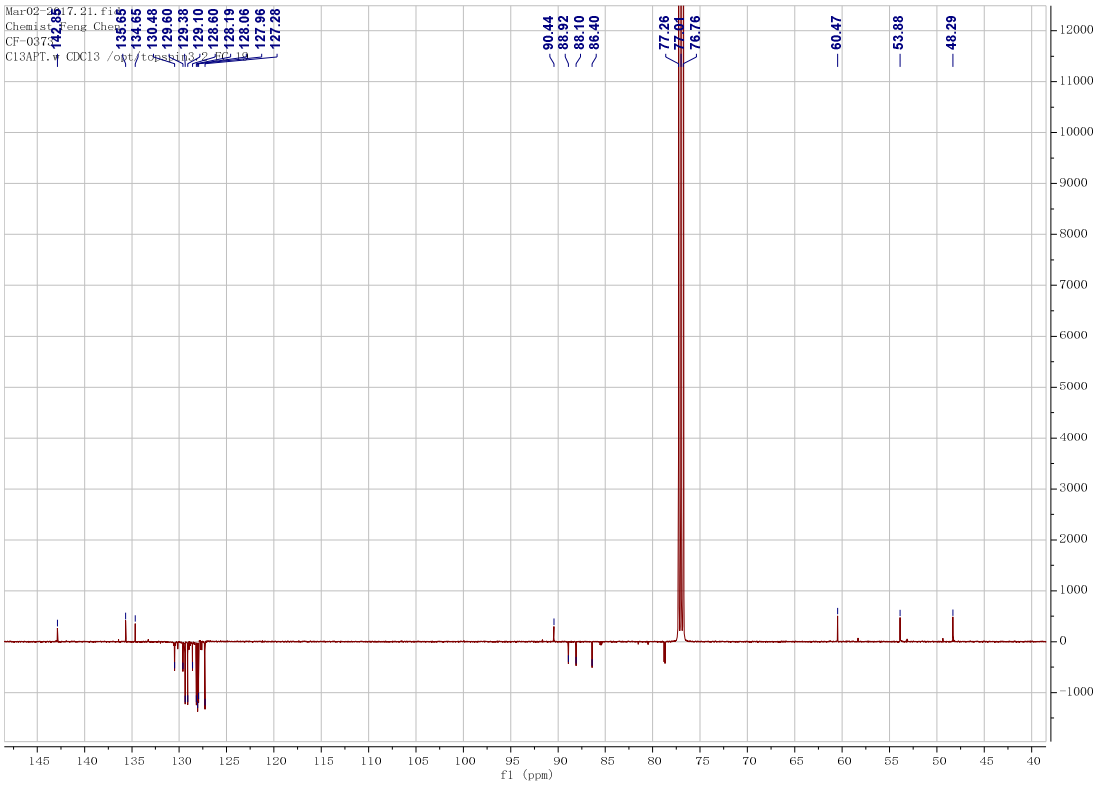

Figure S15. ^{13}C NMR spectrum of complex **7**

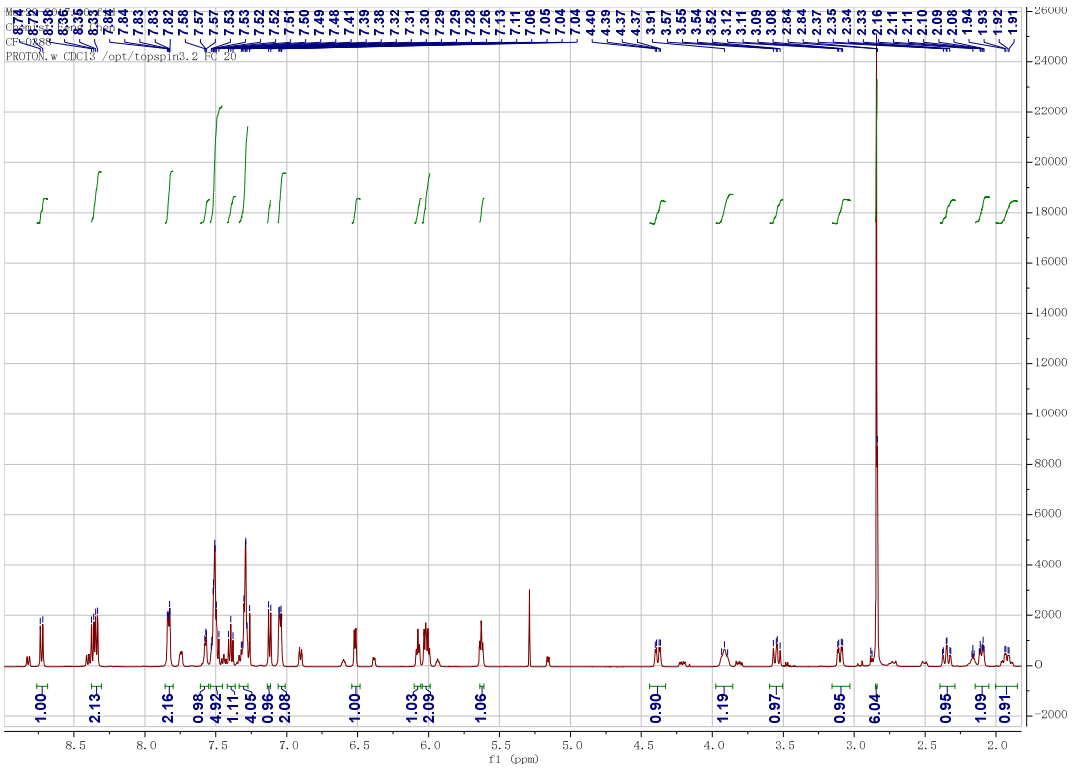

Figure S16. ^{1}H NMR spectrum of complex **8**

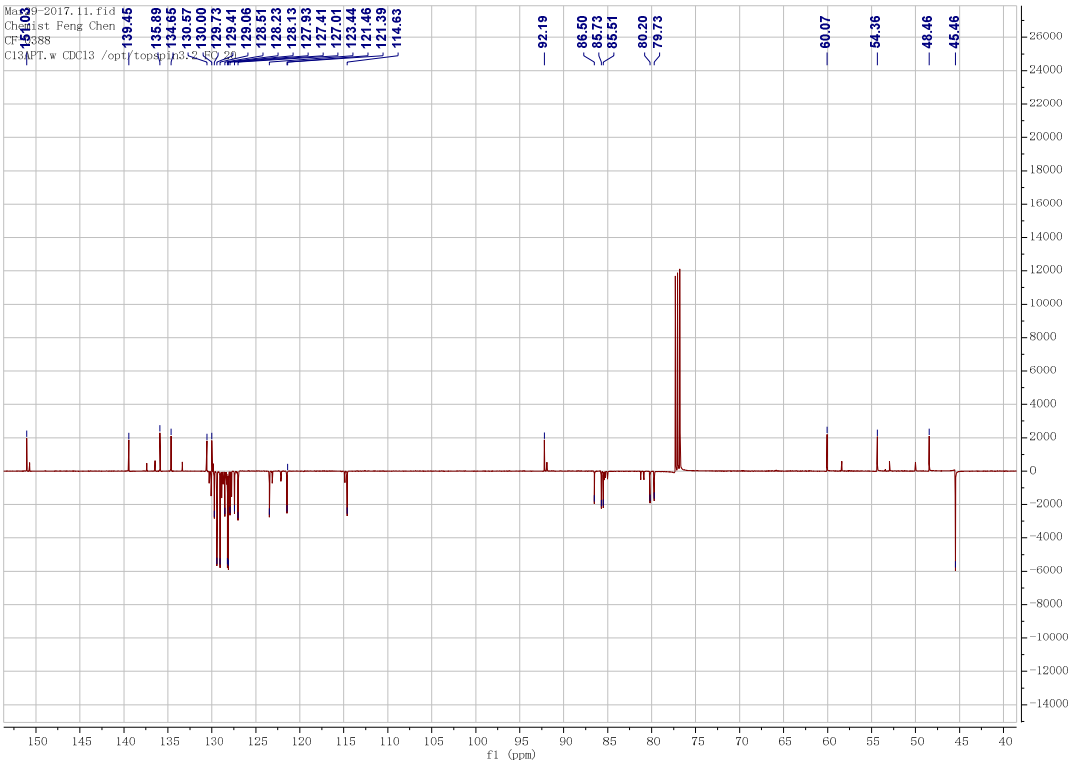

Figure S17. ^{13}C NMR spectrum of complex **8**

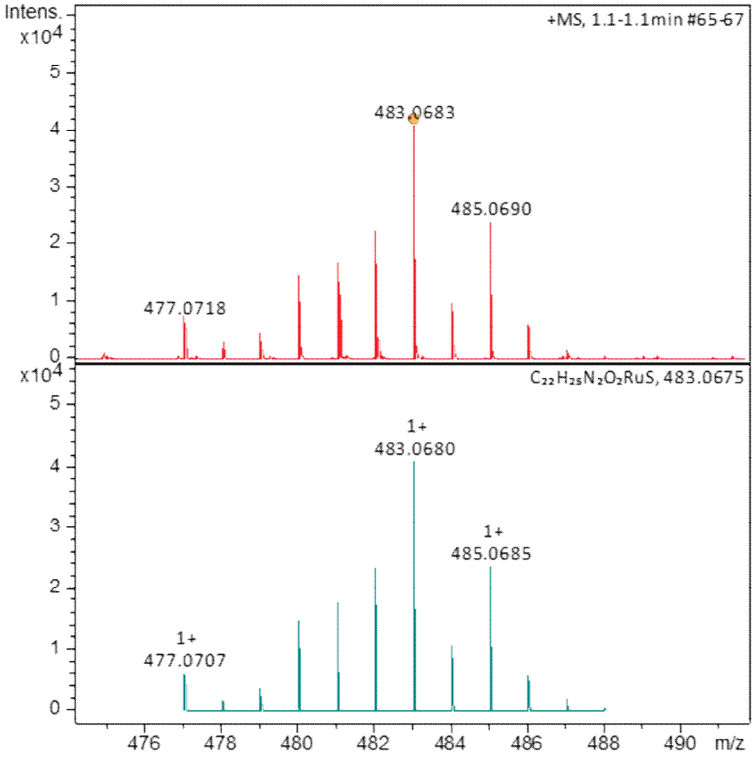

Figure S18. HRMS spectrum of complex **1**; top: acquired data, bottom: simulated data.

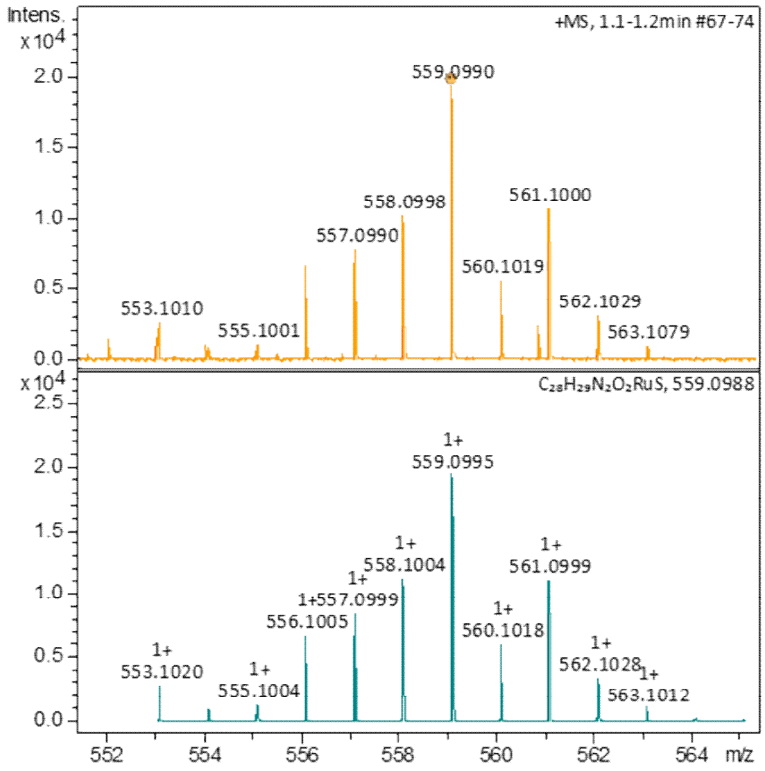

Figure S19. HRMS spectrum of complex **2**; top: acquired data, bottom: simulated data.

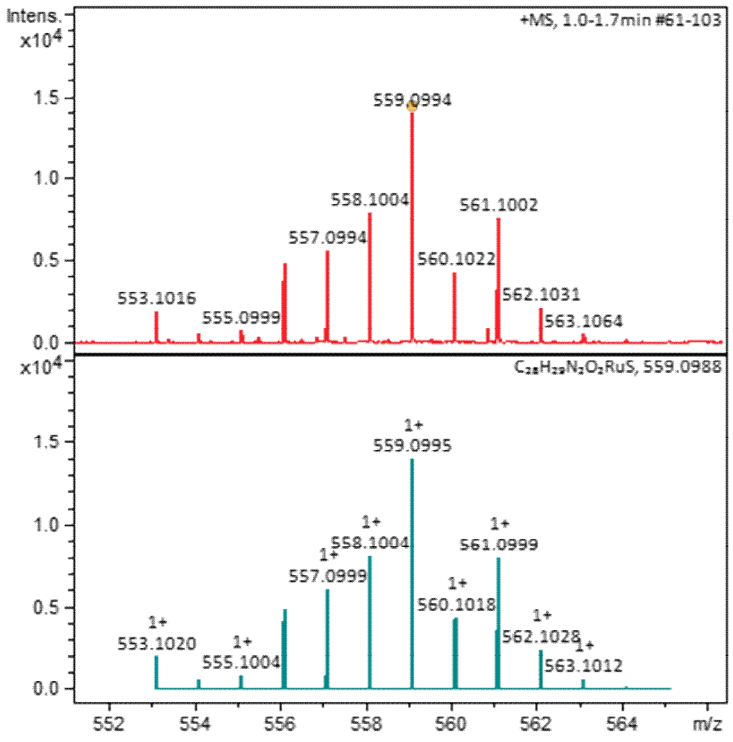

Figure S20. HRMS spectrum of complex **3**; top: acquired data, bottom: simulated data.

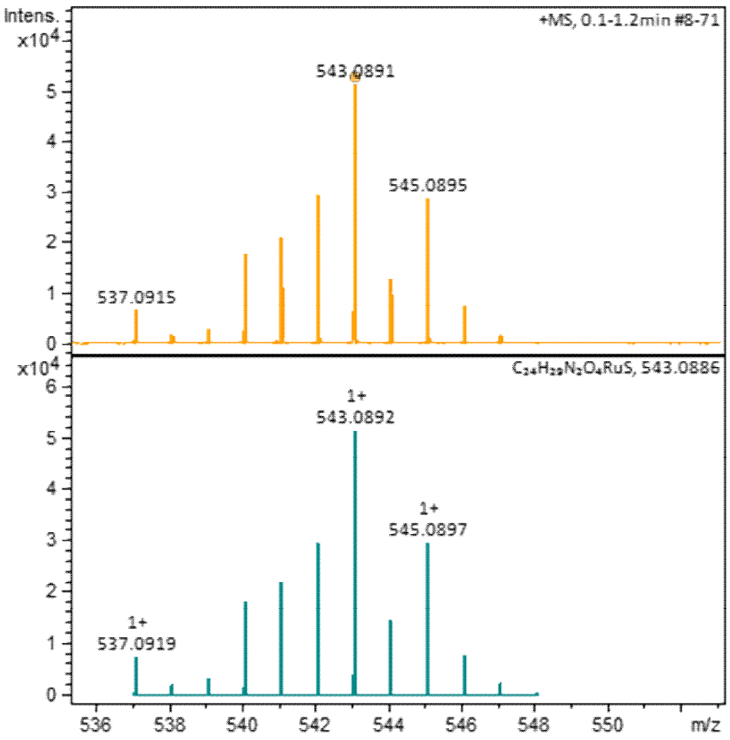

Figure S21. HRMS spectrum of complex **4**; top: acquired data, bottom: simulated data.

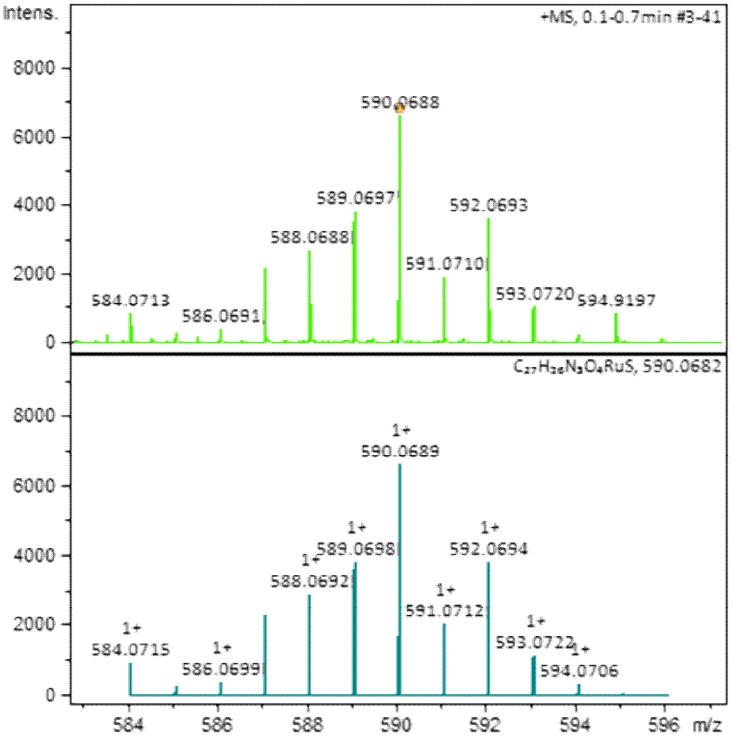

Figure S22. HRMS spectrum of complex **5**; top: acquired data, bottom: simulated data.

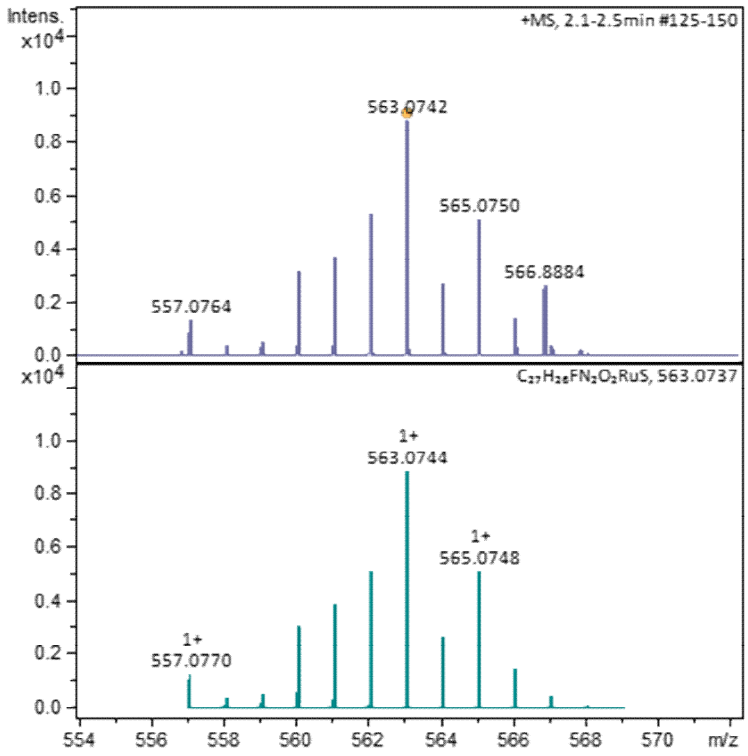

Figure S23. HRMS spectrum of complex **6**; top: acquired data, bottom: simulated data.

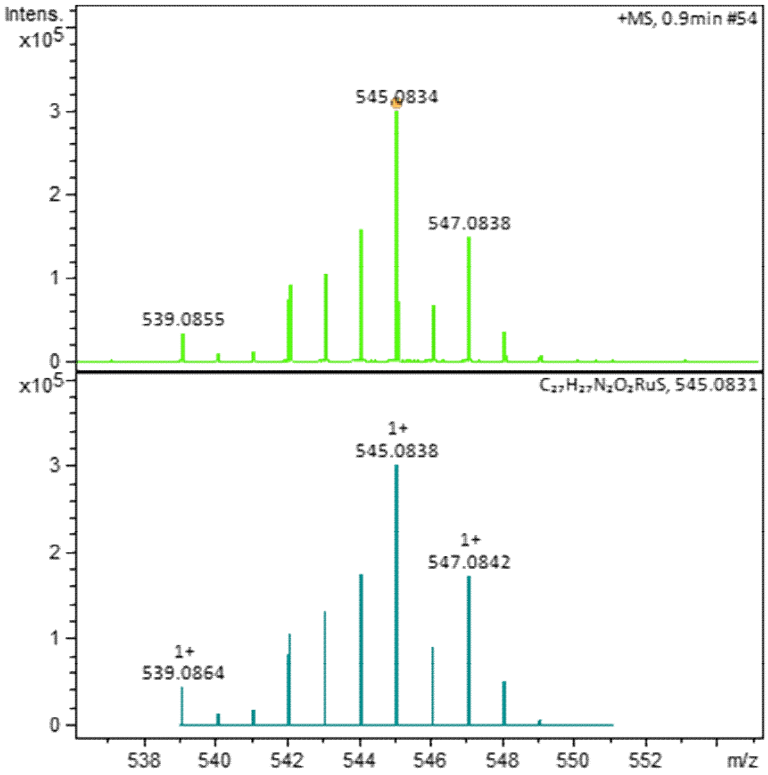

Figure S24. HRMS spectrum of complex **7**; top: acquired data, bottom: simulated data.

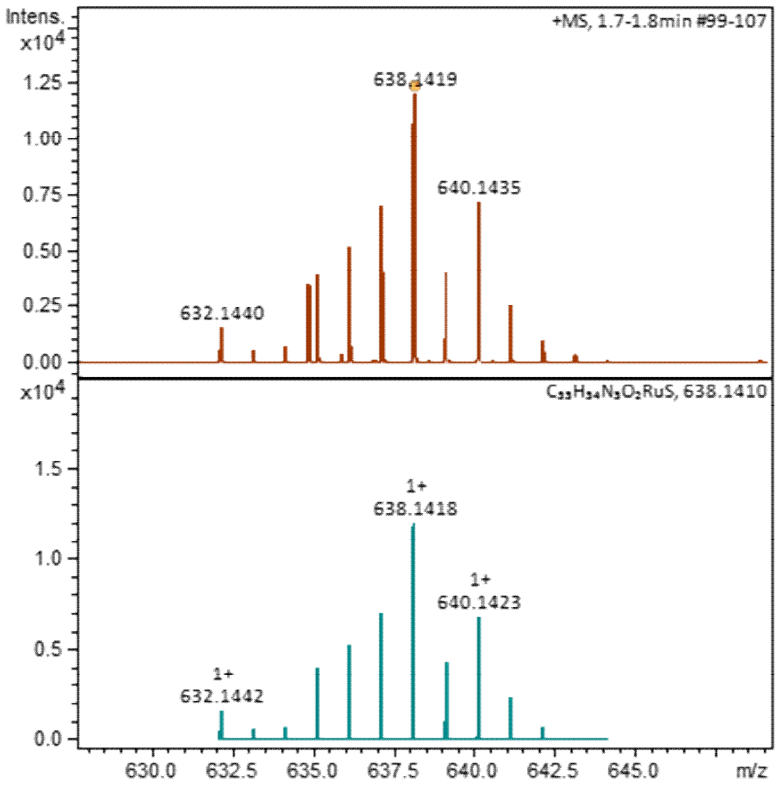

Figure S25. HRMS spectrum of complex **8**; top: acquired data, bottom: simulated data.

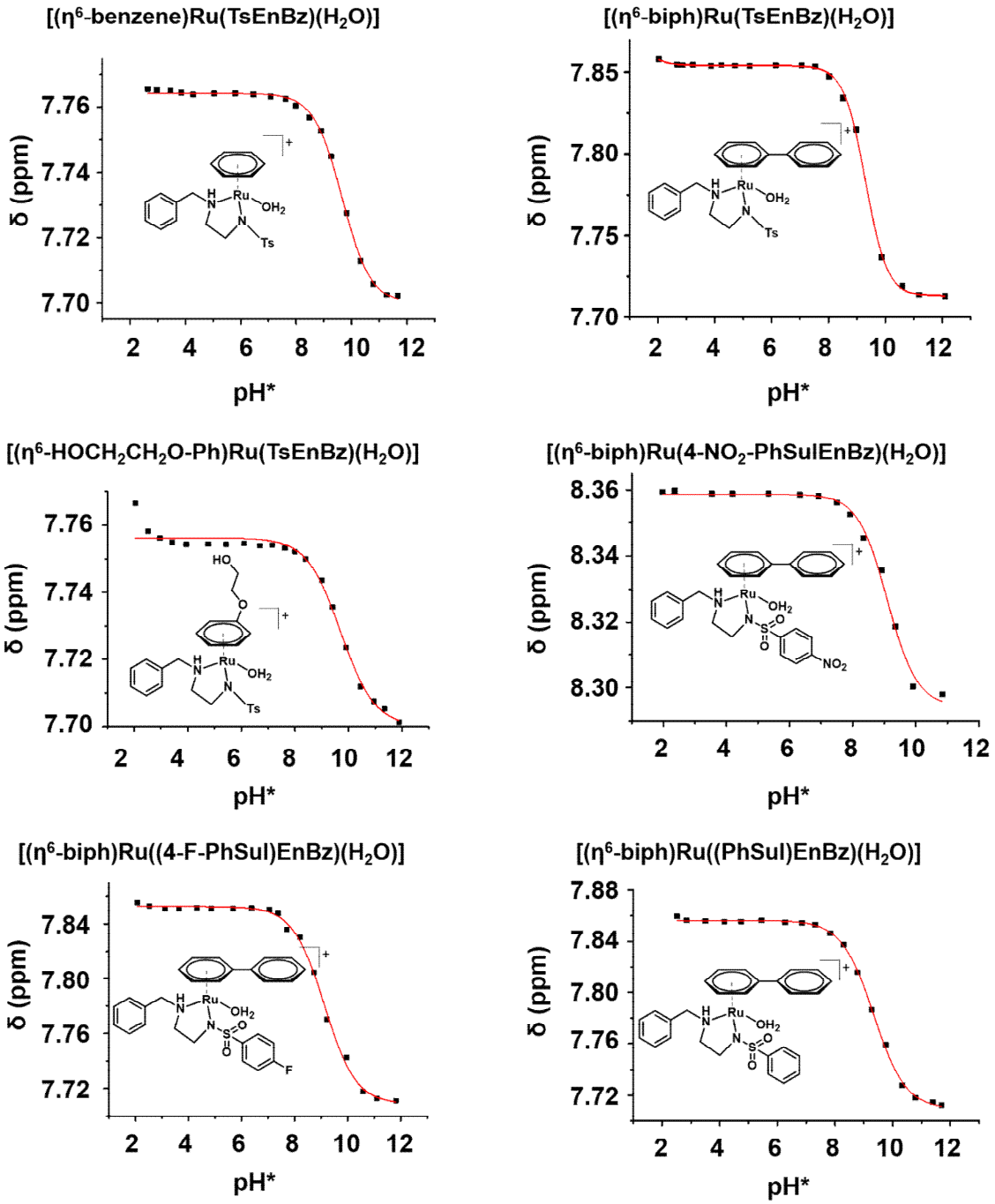

Figure S26. Dependence of NMR chemical shifts of the arene protons of aqua species of complexes **1**, **2** and **4-7** on pH*. The lines (red) were fitted to Henderson-Hasselbalch equation with the pK_a* values shown in Table 3.

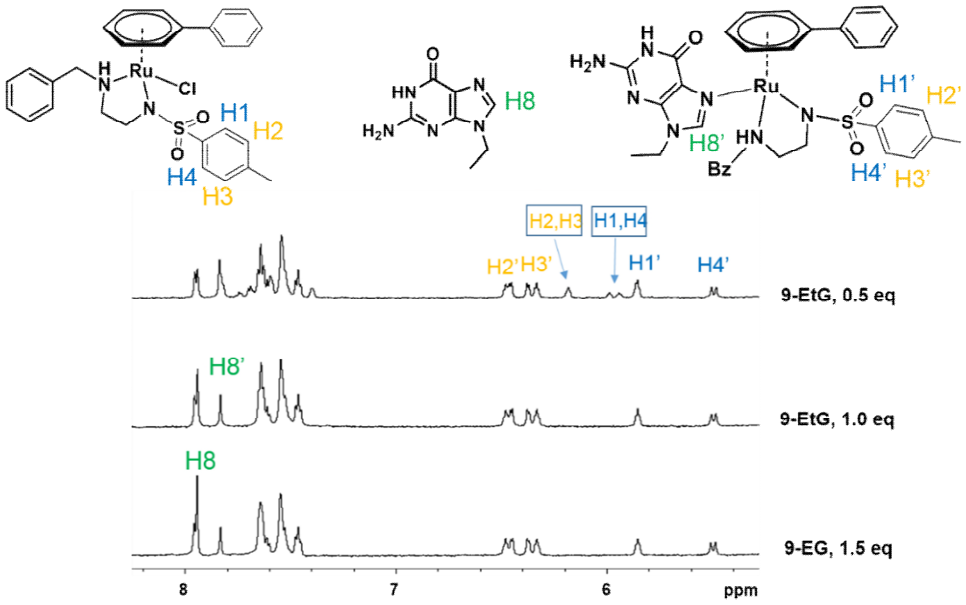

Figure S27. Low field region of ^{1}H NMR spectra for titration of complex **2** (2 mM) with 9-ethylguanine (9-EG, 1 mM – 3 mM, 0.5 – 1.5 mol equiv) in 10% MeOD-d_4/90% D_2O, pH* 7.2, 310 K. Blue arrows correspond to unreacted Ru complex.

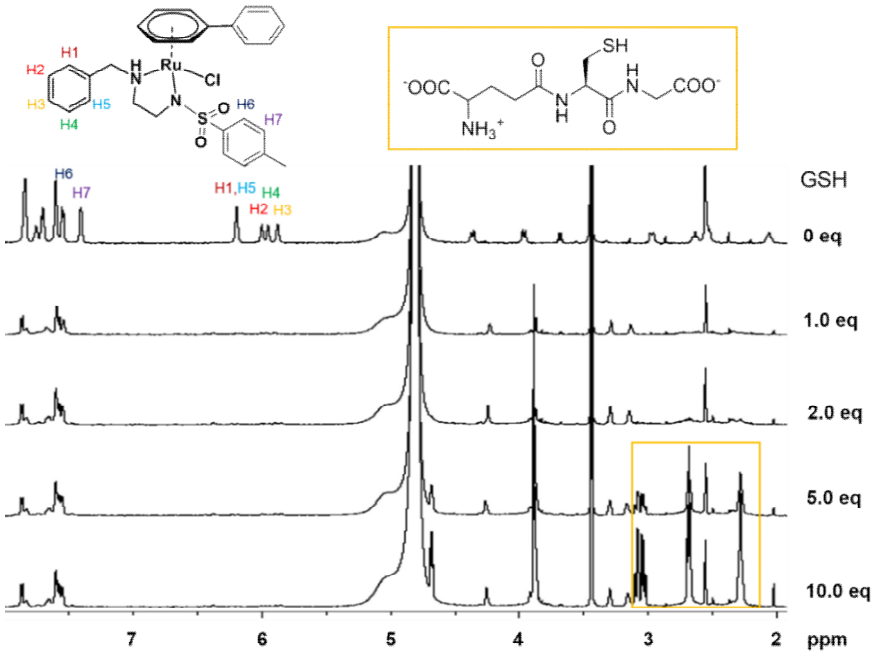

Figure S28. ^{1}H NMR spectra (600 MHz) for reactions between complex **8** and various concentrations of GSH (1.0-10 mol equiv) in MeOD-d_4 and D_2O (2:8, v/v). The pH* was adjusted to 7.2 ± 0.1 and all spectra were recorded at 310 K. Peaks for unreacted excess GSH are in the orange box.

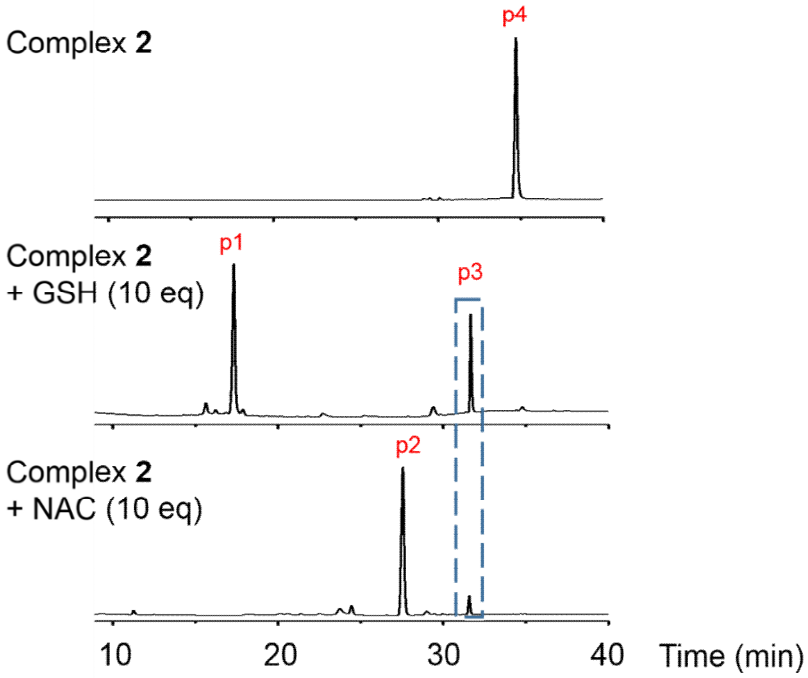

Figure S29. HPLC chromatograms for reactions of complex **2** with GSH or NAC monitored at 254 nm. Solutions of complex **2** (2 mM, MeOH/H_2O, 1:9 (v/v)) with GSH or NAC (20 mM, H_2O) were pre-incubated for 24 h at 310 K. pH values of the solutions were adjusted to 7.2 ± 0.1. Column: ZORBAX Eclipse XDB-C18, 9.4 × 250 mm, 5 µm; eluent gradients, acetonitrile%(min): 2%(0), 12%(10), 15%(15), 25%(25), 50%(30), 50%(50), 2%(55); trifluoroacetic acid (TFA) was used to optimise the shape of the peak. Peak assignments are shown in **Table S3**.

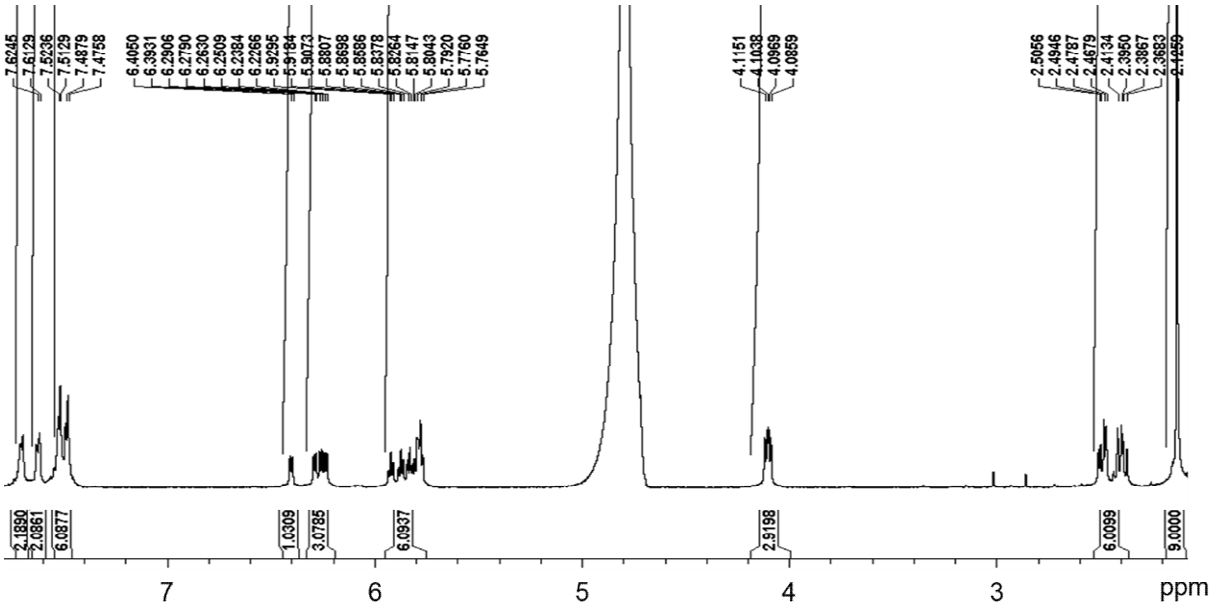

Figure S30. ^{1}H NMR spectrum of $[(\eta^6\text{-biph})_2Ru_2(NAC\text{-}H)_3]^{2-}$, complex **2b**.

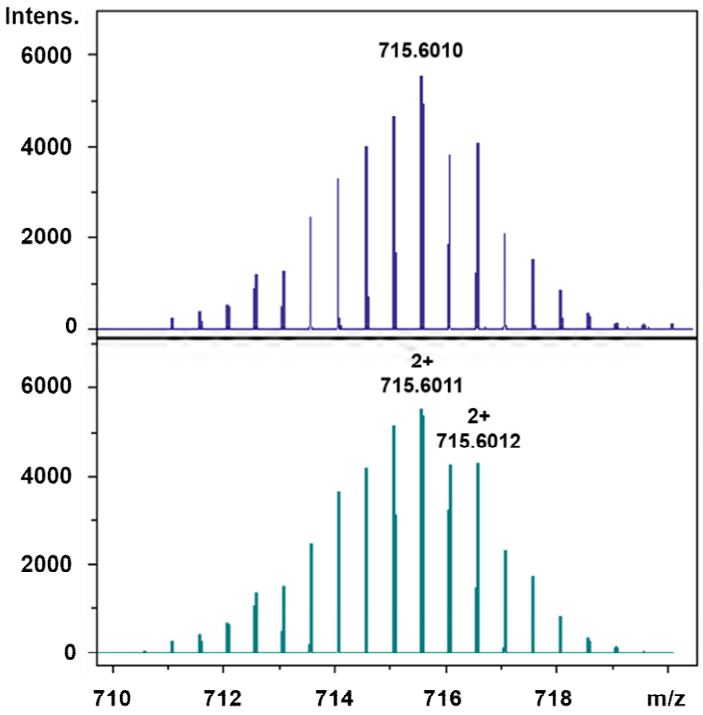

Figure S31. High resolution mass spectrum for $[(\eta^6\text{-biph})_2Ru_2(GS)_3+4H]^{2+}$ assignable to complex **2a** $[(\eta^6\text{-biph})_2Ru_2(GS)_3]^{2-}$; top: acquired data, bottom: simulated data.

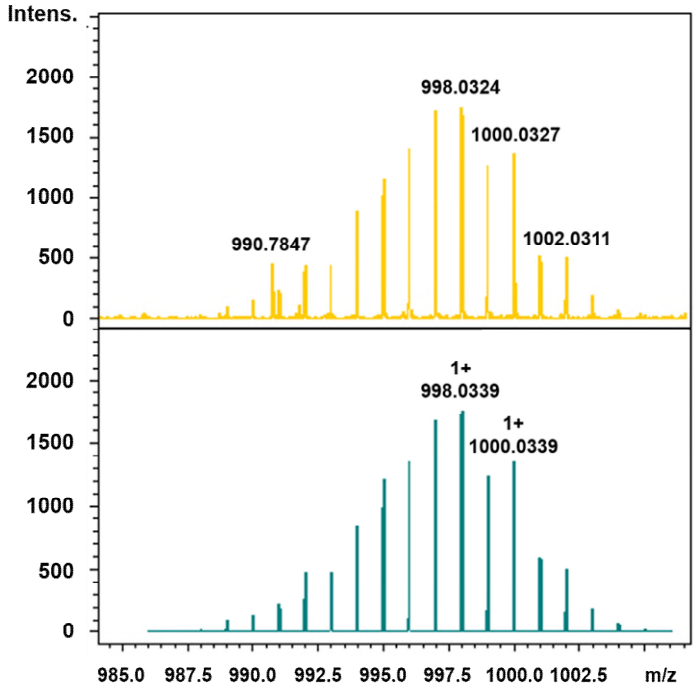

Figure S32. High resolution mass spectrum for $[(\eta^6\text{-biph})_2Ru_2(NAC)_3]^{+}$ assignable to complex **2b** $[(\eta^6\text{-biph})_2Ru_2(NAC\text{-}H)_3]^{2-}$; top: acquired data, bottom: simulated data.

Reference

1. F. Chen, J. J. Soldevila-Barreda, I. Romero-Canelón, J. P. C. Coverdale, J.-I. Song, G. J. Clarkson, J. Kasparkova, A. Habtemariam, V. Brabec, J. A. Wolny, V. Schünemann, P. J. Sadler, *Dalton Trans.*, 2018, **47**, 7178–7189.